



**HAL**  
open science

## Seismic hazard on the French Riviera: new data, interpretation and simulations

F. Courboulex, C. Larroque, Anne Deschamps, C. Kohrs-Sansorny, C. Gélis,  
J.-L. Got, J. Charreau, J.-F. Stéphan, N. Béthoux, J. Virieux, et al.

► **To cite this version:**

F. Courboulex, C. Larroque, Anne Deschamps, C. Kohrs-Sansorny, C. Gélis, et al.. Seismic hazard on the French Riviera: new data, interpretation and simulations. *Geophysical Journal International*, 2007, 170 (1), pp.387-400. 10.1111/j.1365-246X.2007.03456.x . insu-00342713

**HAL Id: insu-00342713**

**<https://insu.hal.science/insu-00342713>**

Submitted on 3 Mar 2021

**HAL** is a multi-disciplinary open access archive for the deposit and dissemination of scientific research documents, whether they are published or not. The documents may come from teaching and research institutions in France or abroad, or from public or private research centers.

L'archive ouverte pluridisciplinaire **HAL**, est destinée au dépôt et à la diffusion de documents scientifiques de niveau recherche, publiés ou non, émanant des établissements d'enseignement et de recherche français ou étrangers, des laboratoires publics ou privés.

# Seismic hazard on the French Riviera: observations, interpretations and simulations

F. Courboux,<sup>1</sup> C. Larroque,<sup>1</sup> A. Deschamps,<sup>1</sup> C. Kohrs-Sansorny,<sup>1</sup> C. Gélis,<sup>1</sup> J. L. Got,<sup>2</sup> J. Charreau,<sup>1</sup> J. F. Stéphan,<sup>1</sup> N. Béthoux,<sup>1</sup> J. Virieux,<sup>1</sup> D. Brunel,<sup>1</sup> C. Maron,<sup>1</sup> A. M. Duval,<sup>3</sup> J-L. Perez<sup>3</sup> and P. Mondielli<sup>4</sup>

<sup>1</sup>Géosciences Azur, Nice Sophia-Antipolis University, CNRS, Paris 6 University, IRD, 250 av Einstein, 06560 Valbonne, France.

E-mail: courboux@geoazur.unice.fr

<sup>2</sup>LGIT, Université de Savoie, 73376 Le Bourget du Lac, France

<sup>3</sup>CETE Méditerranée, ERA risque sismique, 56 bd Stalingrad, 06300 Nice, France

<sup>4</sup>Direction environnement urbanisme et construction, Principauté de Monaco

Accepted 2007 March 28. Received 2006 December 22. in original form 2005 October 20

## SUMMARY

We present here a detailed analysis of a seismic data set recorded by a dense seismological network installed over 6 months in the southeast of France. This experiment was set-up at the boundary between the Ligurian basin and the southern subalpine thrust belt (the Nice arc), which is a complex tectonic region that undergoes low to moderate seismicity. We recorded more than 500 microearthquakes, among which 348 occurred exactly in the centre of the network during a very active seismic sequence that lasted mainly over 2 months.

We performed an absolute location of all of the events and calculated the magnitudes. Then we applied a cross-correlation technique to gather similar events and to relocate relatively few of them. This method revealed a very clear alignment of 19 events in a direction N120° oblique to the N20° general trend of seismicity. Focal mechanisms were determined for the four largest events and composite solutions for 32 smaller ones. Both the alignments of the earthquakes and the focal solutions revealed that two oblique segments of the fault were activated during the crisis.

The main segment (8 km long) that was oriented NNE with a left-lateral strike slip movement is called the Blausasc fault. Taking into account the tectonic evolution and the relationships between surface structures and the distribution of earthquakes, and through a paleoreconstruction of the tectonic evolution, we propose that the Blausasc fault is the hidden root of the Peille-Laghet fault, which has a mapped length of at least 15 km. The smaller segment (0.6 km long) that was activated during the crisis could be interpreted as an antithetic Riedel fracture.

The active Blausasc fault is located in a densely populated zone, at only 10 km from the crowded cities of Monaco and Nice. It is thus particularly interesting to analyse it for hazard assessment. In the last section, we present a simulation that is aimed at predicting what the ground motion in the city of Nice would be like if an earthquake of magnitude 5.7 occurs on this fault. For this, we used the recordings of the largest event of the seismic sequence ( $M_l = 3.2$ ) and an empirical Green's function summation scheme to simulate the ground motion at two stations situated in urban environments. The values obtained show that especially on soft soil sites, the effects of such an earthquake would be considerable in the city of Nice.

**Key words:** earthquake location, earthquake-source mechanism, fault tectonics, microseismicity, seismotectonics, strong ground motion.

## 1 INTRODUCTION

The southeast of France (Fig. 1) is a region where the seismicity is low to moderate. It is an area where we can record daily

microseismicity, and about every 5 yr there is an earthquake of magnitude 4.5–5 that is felt by the population without causing real damage. In this context, is it particularly important to study the seismic potential of this region? The answer is yes, because large

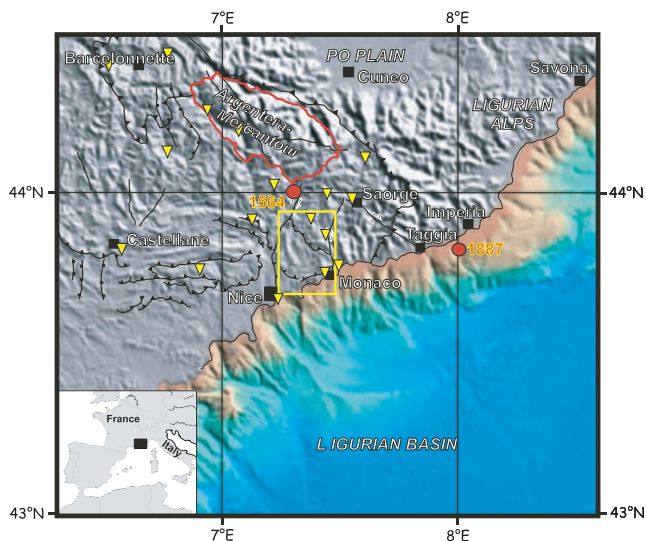


**Figure 1.** Topographic and bathymetric representation of the Alps–Ligurian basin junction. The northern Ligurian continental margin and the deep oceanic Ligurian basin (data from IFREMER) are in colour, and the onshore domain is in shaded grey (data from GT0P030). The Nice area is surrounded by the Castellane arc to the west, the Nice arc and the Argentera-Mercantour massif (red line) to the North and the Ligurian oceanic basin to the south. The major faults are in black and the yellow rectangle is the location of Fig. 3. The green triangles represent the stations of the permanent seismic networks in 2001. The yellow dots are the macroseismic epicentres of the two major historical earthquakes. Inset: relative location of Fig. 1 in the western European surrounding.

destructive earthquakes have occurred in this region in the past. During the XVI century, one or two seismic events destroyed numerous villages just inland from Nice (Working Group CPTI 1999; Larroque *et al.* 2001). Their magnitudes and locations cannot be established precisely, but the damage they caused is mentioned in many documents. More recently, in 1887, an earthquake of an estimated magnitude of 6.5 (Ferrari 1991; Eva & Rabinovich 1997; Scotti & Levret 2000; Bakun & Scotti 2004) occurred offshore, within a few kilometres of the Italian Ligurian coast. This earthquake killed hundreds of people.

These destructive events demonstrate that the seismic hazard in this zone should not be neglected, and they justify a precise study for a better definition of its seismogenic potential. If we consider the high density of population on the French Riviera and its constant expansion, it appears that the seismic risk has to be seriously taken into account in this area.

Even if western European countries are considered as areas of low to moderate seismicity, the permanent and temporary seismic networks allow recording of significant organized seismic activity, even in France (Pauchet *et al.* 1999; Souriau *et al.* 2001; Thouvenot *et al.* 2003; Perrot *et al.* 2005). In our region of interest (Fig. 1), the permanent network is quite dense and allows the location of most of the earthquakes of magnitudes equal to or larger than 2. Nevertheless, seismicity maps that are obtained with these earthquake locations appear very diffuse, and have not enabled us to distinguish any alignments of events that can clearly highlight the activity of faults (Fig. 2a). Therefore, the location, geometry and seismogenic potential of active faults are poorly described in this region, which makes it difficult to estimate the seismic hazard.

To obtain better precision in microearthquake location and a better idea of the active segments of faults, we installed over a 6-month period a very dense seismic network in a small zone that was suspected

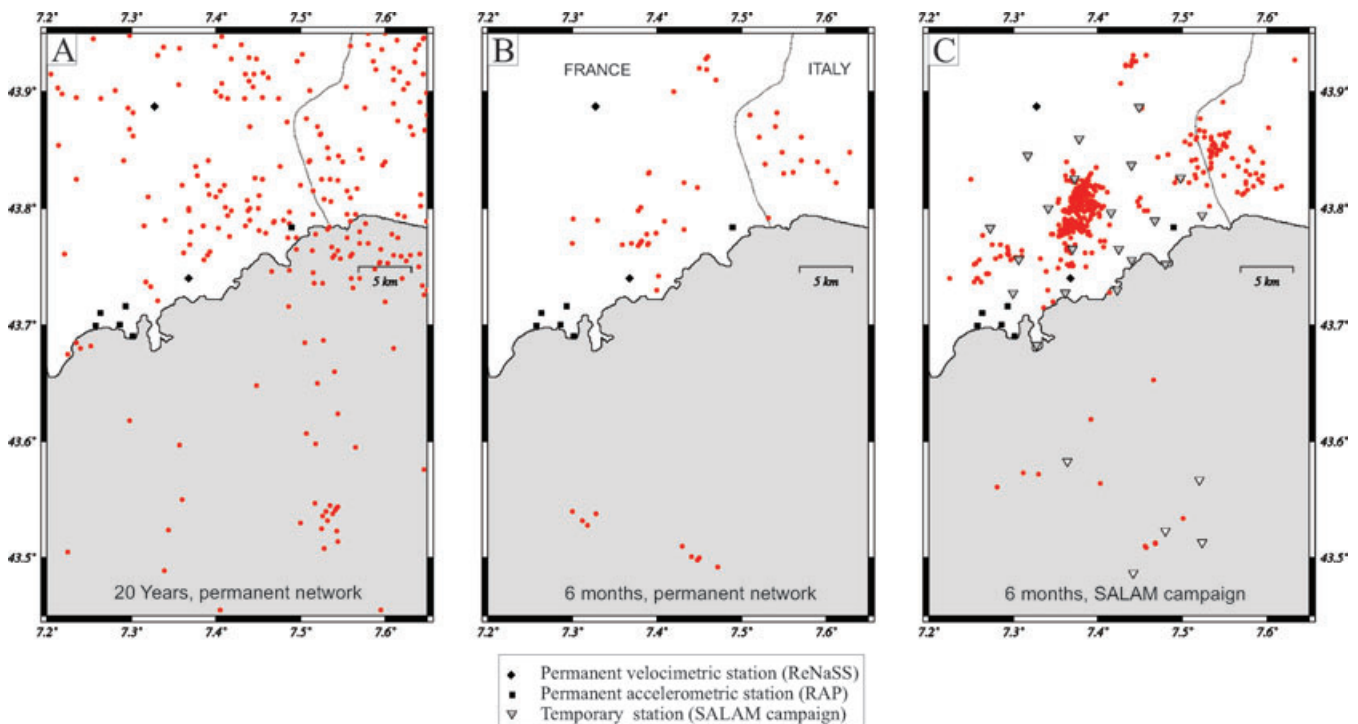


**Figure 2.** (a) The seismicity detected by the permanent seismic network (ReNaSS) over 20 yr (February 1980–October 2000), (b) over 6 months (October 2000–April 2001), the SALAM period and (c) the seismicity detected by the temporary dense SALAM network (October 2000–April 2001). Triangles are the onshore and OBS stations of the SALAM network, squares and diamonds are the stations of RAP (Réseau Accélérométrique Permanent) and ReNaSS (Réseau National de Surveillance Sismique) permanent networks, respectively.

of being active. This work was completed with a morphotectonic investigation in the field, from aerial photographs and satellite images.

During the SALAM period (October 2000–April 2001), three areas were particularly active (Fig. 2c): a small zone inland (15 km north of the city of Nice) in the centre of the seismological network experienced a seismic crisis that will hereafter be referred to as the Blausasc sequence; an offshore zone (25 km south of the city of Nice) where an earthquake of magnitude  $M_l = 4.6$  occurred; and an eastern zone in Italy. Here, we focus on the first zone and present the new seismological and geological data that have been collected along with their analysis using different methods. We show that the inland seismicity during this period revealed clear alignments, and we try to establish their link with the traces of faults and the geological evolution of the area. We then take advantage of the new data collected during this period to simulate a hypothetical larger earthquake on the same fault and its recording in the city of Nice, using an empirical Green's function summation method.

## 2 TECTONIC AND SEISMOTECTONIC CONTEXT

### 2.1 Regional tectonic setting

The Nice area is a complex topographical and geological junction between an onshore domain, the southern French Alps, and an offshore domain, the Ligurian basin (Fig. 1). The southern French Alps are made of the high elevation massif of the Argentera and the southern subalpine massifs (the so-called 'arc de Nice' and 'arc de Castellane'). The Argentera massif is a remnant of the Variscan orogen situated along a margin of the old European platform (Ferrara & Malaroda 1969). It is now the southwestern-most external crystalline massif of the Alps, extending 50 km in a NW–SE direction at 80 km from the coast. The subalpine massifs correspond to the Meso-Cenozoic sedimentary cover that was deposited above the basement of the Argentera on the northern Tethyan margin (e.g. De Graciansky *et al.* 1989).

During the last hundred million years, the kinematic evolution of the western European margin has been dominated by the convergence between the Eurasia and Africa plates, which led to the subduction of the Tethyan ocean and then the collision between the continental blocks (Dercourt *et al.* 1986; Dewey *et al.* 1989). Crustal shortening started in the southwestern Alps from around 20 Ma up to the present day, uplifting part of the Variscan basement and leading to the Argentera massif emplacement (Tricard 1984). These deformations also involved the sedimentary cover, which was thrust into a more external position, where it now forms the southern subalpine massifs (Riccou & Siddans 1986). The Castellane and Nice arcs are composed of a series of south-verging fold and thrusts involving the raising of the Mesozoic to Palaeogene sediments above a basal décollement zone in the upper Triassic evaporites.

In the southern French Alps, before the major neogene compressional alpine phase, the basement and sedimentary cover underwent extensional phases of deformation from the early Jurassic up to the Cretaceous (Dardeau 1988). These synsedimentary extensional phases reactivated hercynian faults with NNE–SSW and NNW–SSE trends in the basement (Arthaud & Matte 1975). De Graciansky & Lemoine (1988) proposed that the early Cretaceous extensional faulting in this part of the European continent was related to the opening of the Atlantic Ocean.

East of the Nice arc, the Italian Liguria province corresponds to the internal alpine nappes (Malaroda *et al.* 1970; Bogdanoff *et al.* 2000). Thick helminthoides flysch series of Cretaceous age were

thrust southwestward during the Cenozoic (Kerckhove 1969). Moderate seismicity has also been reported (Bossolasco *et al.* 1972; Madeddu *et al.* 1997; Eva & Solarino 1998) and, for instance, the Saorge-Taggia fault appears to be one of the major active structures (Hoang-Trong *et al.* 1987; Marini 1987; Larroque *et al.* 2001).

Offshore, the present-day western Mediterranean setting results from an incomplete collision between the Africa and Eurasia plates. The narrow Ligurian oceanic basin (Rollet *et al.* 2002) opened during the convergence between the two plates: the continental rifting started at 30 Ma and led to the anticlockwise rotation of the Corsica-Sardinia continental block and to the oceanic spreading in the centre of the basin. The extension ended at 16 Ma (Montigny *et al.* 1981; Edel *et al.* 2001).

Therefore, the southern Alps–Ligurian basin junction is a particularly complex geological domain with a strong tectonic inheritance, large cumulated deformations, and a major continent–ocean boundary. Several of these structures could be reactivated in the present-day state of stress.

### 2.2 Present-day kinematics and state of stress

The convergence between the Africa and Eurasia plates currently continues at a rate of  $6.2 \pm 0.5 \text{ mm yr}^{-1}$  in a  $N343^\circ \pm 9^\circ$  direction at the longitude of the western Alps, according to the Nuvel-1A plate motion model (DeMets *et al.* 1994). From models based on geodetic data, numerous authors (e.g. Sella *et al.* 2002; Nocquet & Calais 2003) have proposed 30–60 per cent lower convergence velocities in a  $N300^\circ$  to  $N350^\circ$  direction. For this reason, the dynamics of active deformation in the western Alps is often thought to be as a consequence of the Africa–Eurasia collision (Mueller *et al.* 1992; Eva & Solarino 1998). Nevertheless, geodetic data attest that: (1) no significant movement occurs between the Corsica-Sardinia block and the western Alps (Vigny *et al.* 2002; Nocquet & Calais 2003) and (2) the major part of the Africa–Eurasia convergence is accommodated southwards along the Maghrebides boundary. Therefore, the current strain pattern in the western Alps could be mainly controlled by the counter-clockwise rotation of the Adriatic microplate around a pole located in the Po Plain (Calais *et al.* 2002).

From the inversion of microtectonic data, Ritz (1992) and Rebaï *et al.* (1992) proposed that in the southern subalpine massifs the regional stress field was homogenous, with a reverse faulting stress regime ( $\sigma_1$  horizontal with a roughly N–S direction) during the Plio-Quaternary era. Many focal mechanisms have been determined in the last 30 yr (Madeddu *et al.* 1997; Eva & Solarino 1998; Baroux *et al.* 2001). The focal solutions of these earthquakes are homogeneous and allow us to propose that the  $P$ -axes of earthquakes (trend NW–SE to N–S) are near the maximum compressive stress direction (McKenzie 1969). In the southern subalpine massifs, the focal mechanisms of the earthquakes are consistent with a strike-slip faulting stress regime ( $\sigma_2$  vertical and a  $N155^\circ$  trending  $\sigma_1$  axis). Offshore, in the Ligurian basin, Baroux *et al.* (2001) determined a reverse faulting stress regime with a  $N115^\circ$  trending  $\sigma_1$  axis.

### 2.3 Historical and instrumental seismicity

The importance of historical seismicity in the Alpes Maritimes is easy to detect in the many villages inland from Nice, where the occurrence of earthquakes is often mentioned. Over the last thousand years to 1920, the far southeast of France and northwestern Italy experienced 58 historical indexed earthquakes (Larroque *et al.* 2001). At least two of these earthquakes caused many casualties:

the Roquebillière earthquake (1564), and the Ligurian earthquake (1887) that reached an intensity of X MCS (Mercali, Cancani and Sieberg scale; Working Group CPTI 1999; Lambert & Levret 1996). The Ligurian earthquake also produced tsunamis that were seen to have run-up heights of around 1–2 m (Eva & Rabinovitch 1997). Whereas the 1887 Ligurian earthquake was located quite a way offshore, this was not the case for the 1564 event (Fig. 1). Indeed, this latter event was located to the village of Roquebillière (Vesubie Valley) because of the large damage that was seen there, although this damage could be due to site or induced effects, like landslides, phenomena that are still important today. A study by Gauberti (1973) shows that this event also caused important damage in the village of Peille, situated at only 15 km from the city of Nice, in the region of interest of this article. In general, locations of historical earthquakes are not accurate enough to associate them with faults.

The instrumental seismicity that has been gathered since 1960 was more accurately determined from 1976, when the permanent stations of the Réseau National de Surveillance Sismique Français (ReNaSS) network were installed. Now, there is a quite dense seismic network (Fig. 1): 11 short-period stations (six from ReNaSS, four from Sismalp and one from CEA: Commissariat à l'Énergie Atomique); four broad-band stations (ReNaSS-TGRS network) and 10 accelerometers (RAP: Réseau Accélérométrique Permanent) are operating in the Alpes-Maritimes region. Due to this network, an

earthquake of magnitude greater than 4.5 is recorded on average every 5 yr, along with daily microseismicity. The repartition of epicentres enables the highlighting of some major active structures, like the Saorge-Taggia fault (Fig. 1) that is mainly situated in Italy (Hoang Trong *et al.* 1987), and the Argentera-Bersezio fault in the north of the region (Grellet *et al.* 1993), although the majority of the seismicity appears diffuse and not easily related to geological structures. Both inland and offshore, evidence of epicentre alignments are not clear at all, and it is necessary to have a denser seismological network to be able to image precisely the activity of segments of faults. In 1999, an earthquake of magnitude  $M_l$  3.2 occurred at 15 km from the city of Nice. The studies of this event have revealed that it could have been due to a left-lateral fault called the Peille-Laghet fault (Courboux *et al.* 2001). This small earthquake has made us think that this fault could be active, and, because of its proximity to a densely populated area, very dangerous. This is the reason why we decided to further investigate this segment of the fault and installed a dense temporary network during a period referred to as SALAM.

## 2.4 Seismotectonic pattern of the SALAM campaign area

Following the 1999 November 1, Peille earthquake (Courboux *et al.* 2001), the SALAM experiment was installed at the frontal part of the Nice arc (Figs 1 and 3). The Nice arc is a complex tectonic zone

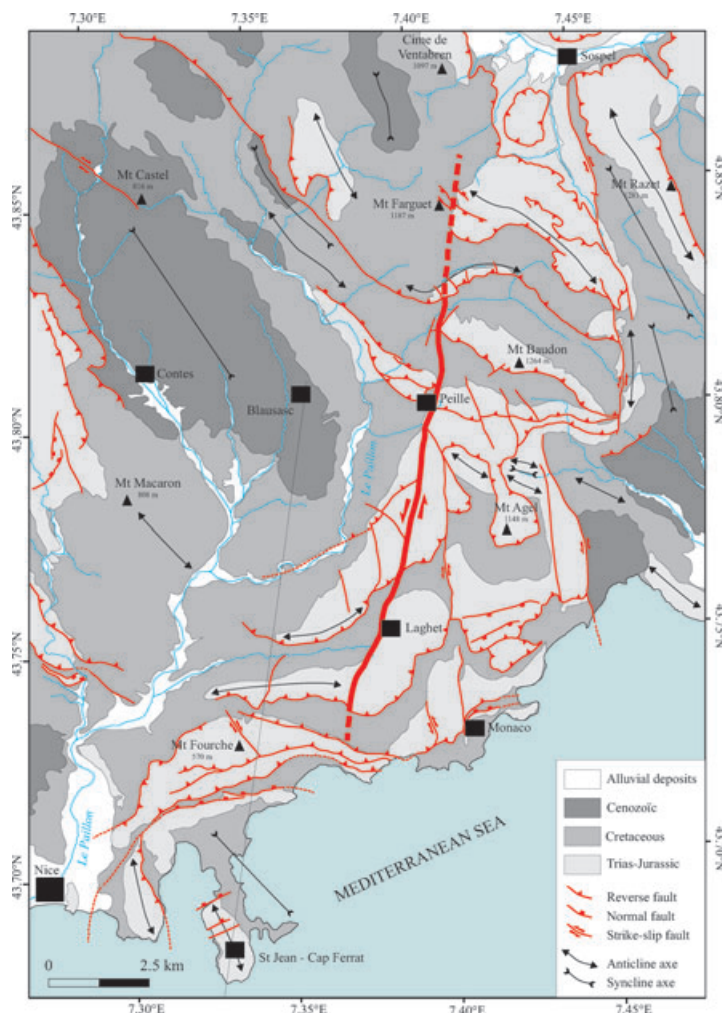


**Figure 3.** Tectonic map of the study area (frontal part of the Nice arc). The Peille-Laghet fault is in bold and the grey line from Blausasc to Saint Jean Cap-Ferrat corresponds to the geological cross-section of Fig. 4.

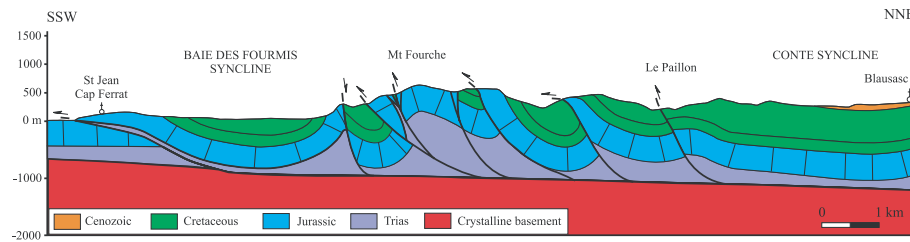


**Figure 4.** Geological cross-section from Blausasc to Cap-Ferrat (see Fig. 3 for location). The frontal part of the Nice arc corresponds to seven imbricate thrust-sheets made of sedimentary rocks from Triassic evaporites (décollement level) up to Cenozoic. At the frontal part of the belt, only the sedimentary cover appears to be thrust up, the crystalline basement is not involved by duplex structures.

with large folds trending NW–SE to E–W (Bulard *et al.* 1975; Perez 1975). These folds are crosscut by numerous south-verging thrust faults and strike-slip fault zones involving series of Mesozoic to Palaeogene sediments. The Nice arc is bounded by two large strike-slip fault zones to the west and east (Fig. 1). Inside these boundaries, the major structures are north-dipping thrusts trending roughly E–W and a NNE–SSW left-lateral strike-slip fault: the Peille-Laghet fault (Fig. 3).

The first compressional deformation started around 20 Ma and produced folding with NW–SE trends. The major alpine compressional phase took place around 8–5 Ma (Gèze 1960; Perez 1975; Riccou & Siddans 1986). The fold and thrust belt was moved southwards, above a décollement zone lying at the base of the sedimentary cover in Triassic evaporites. Below the sedimentary cover, the crystalline basement has undergone deformation since the Palaeozoic, with major hercynian basement structures striking E–W and NNE–SSW (Arthaud & Matte 1975; Debran-Passard *et al.* 1984).

In this area, seismic sections and boreholes do not exist. Therefore, the subsurface structure can only be based on geological knowledge. At the frontal part of the Nice arc, the thickness of the sedimentary rocks that are overlying the basement corresponds to the thickness of the layers from Trias up to Late Cretaceous. Taking into account that the thicknesses do not change significantly on the scale of the frontal belt, we measured the mean thickness of the different layers from the sections provided by river incisions and we propose a value of  $1300 \pm 300$  m. From field data and cartography, we built a geological cross-section from Blausasc up to the coast (Fig. 4). As for the neighbouring Castellane arc (Laurent *et al.* 2000), the frontal part of the Nice arc is an imbricate stack of sedimentary thrust-sheets (Siddans 1979; Malavieille & Ritz 1989). The boundary between the sedimentary cover and the crystalline basement has a northward dip from  $-700$  m under sea level below the Cap Ferrat to  $-1250$  m below Blausasc. We propose that the basement-sedimentary cover interface is smooth because we have no evidence for deep-seated major basement structures and it is consistent with the thickness of the Mesozoic layers. From Blausasc to Cap Ferrat, the imbricate stack is made up of seven thrust sheets; it is bounded to the North and to the South by two major synclines: the Contes syncline and the Baie des Fourmis syncline, respectively.

From striation on fault planes, schistosity direction and fold direction, we determined a mean shortening in a N170° direction during the emplacement of the Nice arc. Unfortunately, it is not possible to build a cross-section according to the shortening direction because of local structural complexity and dense urbanization. Nevertheless, we tried to determine the displacement between Blausasc and the coast using the present-day base of the competent Jurassic limestones as a reference, to unfold the strata along the Blausasc-Cap Ferrat cross-section (Fig. 4). If we consider that the sedimentary cover south of the coastal domain is autochthonous, and taking into

account the angle between the shortening direction and this cross-section, the unfolding of the stratas allows us to propose a range of shortening around 4–5 km along the N170° direction for the frontal part of the belt since 20 Ma. This value is consistent with the shortening calculated in the western part of the so-called Castellane arc (Laurent *et al.* 2000).

### 3 GENERAL RESULTS OF THE SEISMOLOGICAL SURVEY

#### 3.1 Temporary network description

We installed a temporary seismic network that was composed of 20 stations, to complement the permanent network in a small zone (20 km × 20 km). The area covered by the temporary network concerns the eastern part of the French Riviera from the city of Nice to the Italian border (Fig. 2c), including Monaco (two stations). It was centred where the Peille earthquake occurred about a year before (Courboulex *et al.* 2001), close to the well-known Peille-Laghet fault.

All the stations installed were three-component digital recorders (16–24 bit) equipped with individual GPS receivers that ensured accurate time correction. About one third of the stations were equipped with CMG40 broad-band sensors, one third with 5 s Lennartz sensors, and the rest with 2 Hz sensors (L22). All of the stations worked in continuous mode with a sampling frequency of 125 or 200 Hz. The network was operating over a period of 6 months, from 2000 October 16 to 2001 April 24 and detected 582 events that were recorded by at least three stations in the region of interest, as illustrated in Fig. 2.

#### 3.2 First location results

We picked the first arrival time of *P* and *S* waves on waveforms recorded by the temporary and permanent stations. For first locations of the whole data set, we used a simple layered model (Bertil *et al.* 1989). We identified 64 events as quarry blasts and ignored them. To do this, we first collected the carrier's information when possible. Then, we compared the seismicity map obtained during day and night-time periods and cancelled out two swarms of events that systematically occurred during the day around the same times. We believe that most of the artificial shots were removed through this analysis, but we are aware that a few shots may still be present in the catalogue.

Using the HYPOCENTRE code and SEISAN software (Haskov & Ottenmøller 1999), we finally located 518 earthquakes. This is seven times larger than the number of events located by the permanent network (Fig. 5). The usefulness of using a dense seismic network is seen clearly in Fig. 2, where the seismicity recorded by

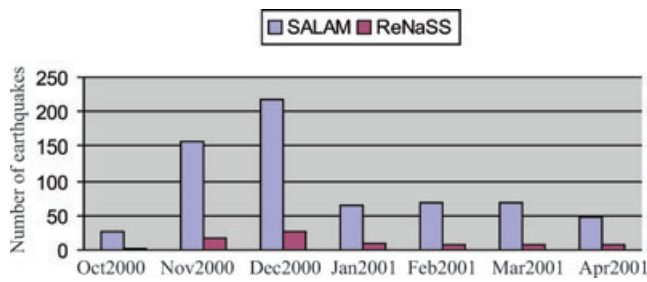


**Figure 5.** Number of earthquakes recorded per month by the permanent and the temporary networks during the SALAM campaign (2000 October 15 to 2001 April 15).

the permanent network over 20 yr (Fig. 2a) and the 6 months of the experiment network (Fig. 2b) are compared with the seismicity recorded by the SALAM network (Fig. 2c). It is obvious from these results that the scarcity of the seismicity maps obtained in this region by the permanent network does not reflect the real microseismic activity. Given the small magnitude of most of the events, the sensitivity of the permanent network does not enable the detection of structural alignments, if they exist.

A first look at the location results (Fig. 6) shows three main zones where the seismic activity was important during these 6 months of the temporary seismic network are as follows.

- (1) A region in Italy that is very close to the France-Italy border.
- (2) A zone situated offshore, where an earthquake of magnitude  $Ml = 4.6$  occurred on 2001 February 25. A more complete study of this event will be the subject of another publication. We only report here, in Table 1, its location using the temporary and permanent networks and its focal mechanism determined from the polarities of direct and refracted  $P$  waves.
- (3) A small zone inland in the centre of the network (around where the Peille event occurred in 1999) where 348 events were located. This crisis, called the Blausasc sequence, is detailed in the present study.

### 3.3 Magnitudes

We searched to determine a local magnitude for the 518 events located, calibrated on the magnitude  $Ml$  calculated by the ReNaSS. Using the 77 events for which magnitudes had been determined by the ReNaSS, we tried to fit the relation:  $\text{Log}(A) - Ml = e \log(D) + f$ , where  $A$  is the maximum amplitude averaged on the three components, high pass filtered at 1 Hz for the broad-band sensors,  $Ml$  is the ReNaSS magnitude, and  $D$  is the hypocentral distance. Because some of our short period sensors did not have precise calibration, we could not properly retrieve the real amplitude at each station, in which case we used directly the rough values. We then obtained the different linear regressions for each station with an almost constant slope  $e$  and various values of  $f$  that account for the instrumental differences between the stations. We carried out different trials with a large number of the stations, and we finally obtained the most stable results using four of the best stations. The relation allows us to propose magnitude estimations for the whole data set, ranging from 0.1 to 4.6 (size of circles in Fig. 6).

### 3.4 Frequency–magnitude relations

The frequency–magnitude distribution (Gutenberg & Richter 1944) describes the power-law relation between frequency of occurrence

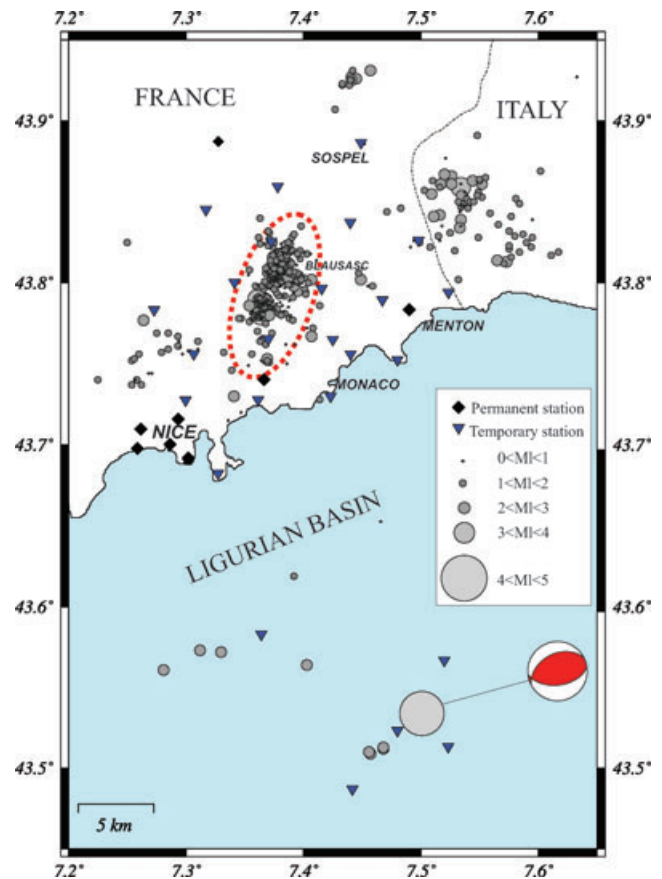


**Figure 6.** Localization and magnitude of the earthquakes recorded during the SALAM seismic experiment. The focal mechanism of the largest earthquake that occurred during the campaign (2001 February 25,  $Ml$  4.6) has been computed using  $P$ -wave polarities on numerous stations. The red ellipse shows the location of the Blausasc sequence.

and magnitude of earthquakes:  $\text{Log } N = a - bM$ , where  $N$  is the cumulative number of earthquakes with magnitudes larger than  $M$ , and  $a$  and  $b$  are constants. We calculated the  $b$  value from the whole data set on the magnitude interval [1.2, 3.4] and obtained a value of 1.08 (Fig. 7a). The linear trend between magnitudes 1.2 and 3.4 indicates that the catalogue is complete for this range of magnitudes. The earthquake of magnitude 4.6 was not taken into account in the  $b$ -value calculation because it is not representative of such a short (6 months) period of seismicity. We show on Fig. 7(a) only the frequency–magnitude distributions obtained using the whole data set, although we also studied the data set that corresponds to the Blausasc sequence only, and the data set without the Blausasc sequence. The  $b$  value we obtained was in all cases very close to 1.

To have a more general view of the Gutenberg–Richter distribution in the southeast of France for a larger time of observation, we calculated the  $b$  value on 20 yr of seismicity recorded by the ReNaSS permanent network in a much larger area (Fig. 7b). The  $b$  value obtained is a little higher (from 1.1 to 1.2), calculated over the magnitude interval [2–4.3]. Magnitudes higher than 4.3 were not taken into account, the time period being certainly too short in comparison with the frequency of occurrence of earthquakes of these magnitudes. Assuming that the Gutenberg–Richter is time-independent and valid over the whole range of magnitude, linear extrapolation to higher magnitudes yields a recurrence time of

**Table 1.** Location and focal solutions of the main events that occurred during the SALAM campaign.

Date	Time	Latitude	Longitude	Depth	$M_l$	Strike	Dip	Rake	Reference on figures
2000/12/19	14:20:49	43.788	7.366	2.6	3.2	216	77	15	Event 1 on Fig. 8(a)
2000/12/20	5:45:14	43.790	7.361	2.6	3.0	216	79	10	Event 2 on Fig. 8(a)
2000/12/19	00:52:24	43.780	7.364	2.8	2.9	204	54	37	Event 3 on Fig. 8(a)
2000/12/21	6:35:54	43.790	7.362	2.7	2.4	224	71	23	Event 4 on Fig. 8(a)
1999/11/01 <sup>a</sup>	17:22:33	43.789	7.367	3.0	3.4	209	75	-4	Event 5 on Fig. 8(a)
2001/02/25	18:34:43	43.53	7.48	11.	4.6	243	41	74	Fig. 6

<sup>a</sup>From Courboulex *et al.* (2001).

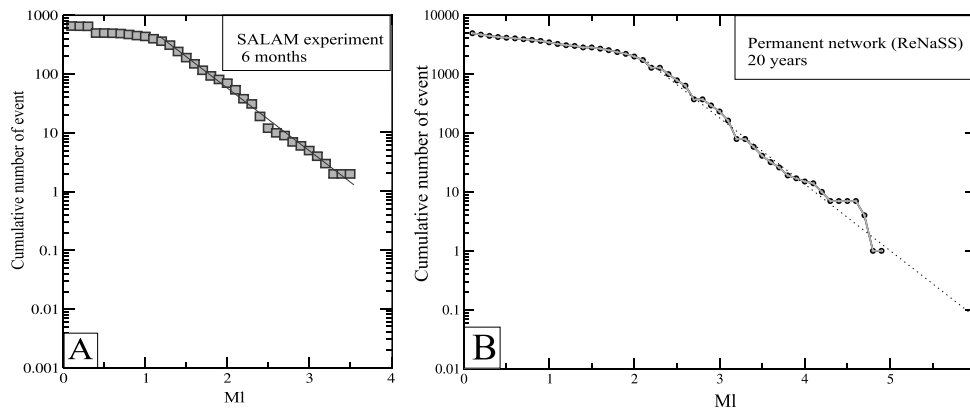


**Figure 7.** (a) Frequency–magnitude distribution of the events detected located during the 6 months of the SALAM experiment (latitude:  $43.5^{\circ}$ – $44^{\circ}$ , longitude:  $7.2^{\circ}$ – $7.7^{\circ}$ ). (b) frequency–magnitude distribution of the events located over 20 yr by the ReNaSS permanent network (latitude:  $43^{\circ}$ – $45^{\circ}$ , longitude:  $6.5^{\circ}$ – $8.5^{\circ}$ ).

200–300 yr for an  $M_l \geq 6.0$  occurring anywhere in the geographical window considered.

It is important to note that to be able to infer anything about the return periods of larger earthquakes from a frequency–magnitude relation, the data set must fulfil the conditions of spatial and temporal stationarity, of completeness to a specified lower magnitude, and of statistical independence. We may consider that 20 yr of observations is a reasonable duration for the magnitudes we chose to study [2, 4.3]. However the conditions of spatial stationarity are subject to discussion in an area where different seismotectonic influences can be superimposed. For this reason, the return period value we obtained for an earthquake of magnitude 6 or more has to be taken cautiously, and only used to remind ourselves that the earthquake hazard of this region is not negligible.

## 4 THE BLAUSASC SEISMIC SEQUENCE

### 4.1 Description of the sequence

One month after the installation of the temporary seismic network, the inhabitants of several villages inland from Nice felt numerous vibrations, especially during the night. Most of the related seismic events were not detected at that time on the permanent network, but we quickly found that the temporary network was sufficiently sensitive to detect these microearthquakes. It was the beginning of a very active seismic sequence that occurred in the centre of our seismic network and so could be recorded with exceptional precision.

The Blausasc sequence mainly lasted from 2000 mid-November to the end of 2000 December, in a small  $8 \text{ km} \times 4 \text{ km}$  area, although it was still active until the end of the full period. We recorded 348 events in this small zone. The main shocks occurred on December 19 and 20, 2000, and were of magnitudes  $M_l$  3.2 and 3.0, respectively.

About 60 events occurred on 2000 December 19, which was the climax of the Blausasc seismic sequence.

These earthquakes were very well felt in the villages close to the epicentre (Blausasc, Peille and Contes) and generated some panic reactions. They were also well felt in the cities of Nice, Monaco and Menton. A macroseismic map published by the Bureau Central Sismologique Français (BCSF) indicated a macroseismic intensity (EMS98) of V in the epicentral zone (data are available on [www.franceseisme.fr](http://www.franceseisme.fr)).

### 4.2 Absolute locations

The absolute locations of the Blausasc seismic sequence have been obtained for 348 events in a very small area (Fig. 8a). To obtain the best 1-D velocity model, we used the VELEST tomographic inversion method with 500 different input models. We found that with our data (many shallow small events in a small zone) this method did not enable us to obtain a better model than the simple initial model we used. Hence, we decided to keep a simple layered model in which velocity raises regularly with depth (Courboulex *et al.* 2003). We also looked for the best  $V_p/V_s$  ratio and found a value of 1.73. We obtained a low average rms of 0.09 s for the events of this zone with a very good azimuthal coverage and a distance to the closest station always smaller than 2.5 km (Fig. 6). The average vertical and horizontal errors raise 1.4 and 1.2 km, respectively.

The earthquakes were very shallow (0–3 km in depth) and were spatially separated into two groups of events by a 1-km-wide gap, with one in the north and the other in the south of the area (Fig. 8a). The epicentres appeared to be aligned on an 8-km-length structure oriented  $N20^{\circ}$ . At depth, events in the north were 1–2.5 km deep and not so well aligned, contrary to the ones in the south, which were deeper and well aligned on a  $70^{\circ}$  dip plane (Fig. 8b). Therefore, we

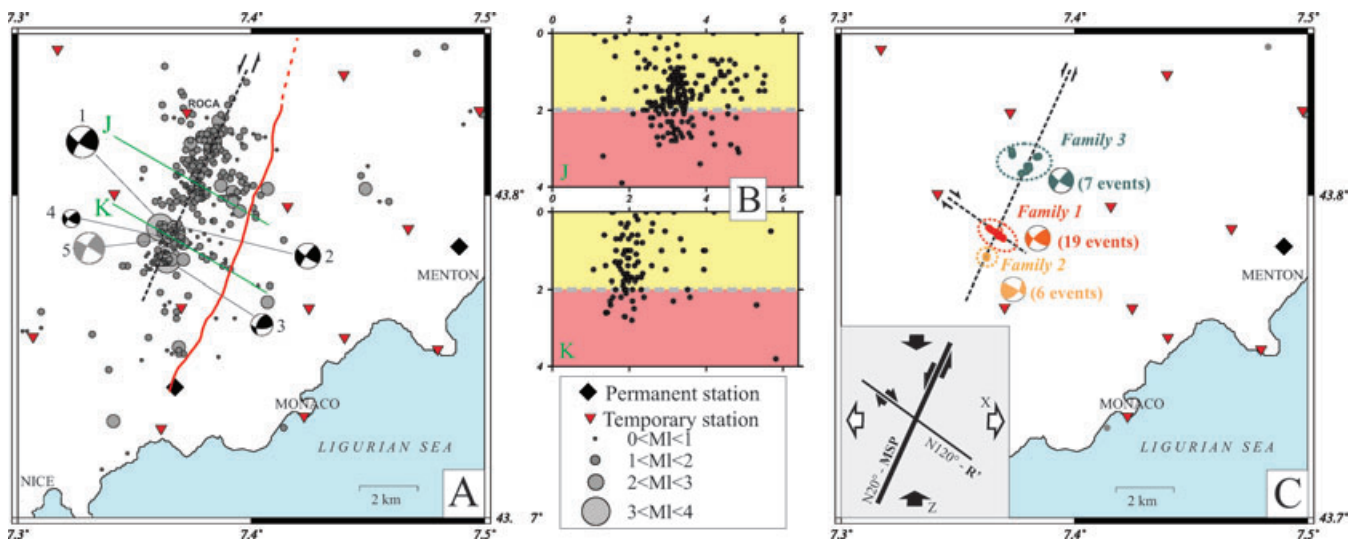


**Figure 8.** (a) Absolute location and magnitude of the earthquakes during the SALAM experiment in the small zone of the Blausasc sequence (grey circles) and individual focal mechanisms of the larger shocks (Numbers refers to Table 1). The red line is the surface trace of the Peille-Laghet fault. (b) Cross-sections (2 km width), the grey dotted line is the maximum depth for the sedimentary cover (yellow)–crystalline basement (red). (c) Relative relocation of the events of three families of multiplets and composite focal mechanism associated. Inset: interpretation of the  $N20^\circ$  and  $N120^\circ$  directions as the main shear plane (MSP) and an antithetic Riedel fracture ( $R'$ ) formed in a simple shear deformation regime;  $Z$ : shortening axis and  $X$ : lengthening axis.

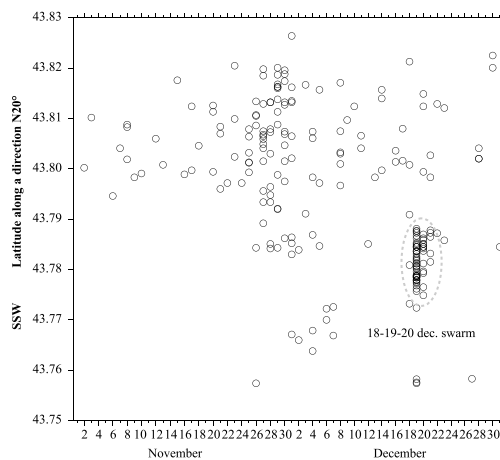


**Figure 9.** Migration of the seismicity from north to south during the Blausasc sequence. The epicentres are projected on a  $N20^\circ$  axis (see Fig. 8).

highlighted the existence of an active fault plane, which we call here the Blausasc fault.

The spatiotemporal distribution of the epicentres showed the migration of the seismic activity from the north in 2000 November to the south in 2000 December (Fig. 9). The two main events took place in the southern part in 2000 December.

### 4.3 Relative relocations using multiplets analysis

To better locate the earthquakes, we performed their relative relocations using the multiplets analysis proposed by Got *et al.* (1994). Given the good distribution of stations around the hypocentres, this method should give reliable results.

First, we created families of similar events by using the cross-correlation of their waveforms. Then, we located events by pairs, transforming time delays into distances. This means that in a family, the events were located towards all other events belonging to the

same family, and not towards one single master event (Fréchet 1985). As a consequence, the event locations were more precise and the shape, azimuth and dip of one family are less sensitive to the velocity model.

Due to this method, we defined three families of events located in three different parts of the fault (Fig. 8c): family 1 (19 events) was located in the centre of the fault segment that was activated during the crisis; family 2 (six events) in the southern part of the segment; and family 3 (seven events) in the northern part. Each of the families was determined with a high cross-correlation value (at least 0.9) on four stations. Only vertical components and  $P$  waves were used in this analysis. As an example, we show  $P$  waves of the 19 earthquakes that belong to family 1 that were recorded on the vertical component of station ROCA (Fig. 10). Even if the station is very close to the epicentres, the waveform is rather similar from one event to the other. Note that the total number of events that could be gathered into families was low (only 32). This is because the earthquakes occurred at shallow depths in a complex velocity medium and are recorded by nearby stations; therefore, the waveforms recorded are complex and not particularly similar to each other. This relocation study will give very precise information on the geometry of small parts of the fault that will complement the already good earthquake repartition we obtained with the absolute location method.

The results of relocation was surprising for family 1 (Fig. 11): a very clear alignment of the 19 events was obtained in a direction  $N120^\circ$ , almost perpendicular to the main elongation of the seismicity along the Blausasc fault. At depth, the events belonging to this family were separated by 300 m at most. Location errors do not exceed 20 m horizontally and 50 m vertically. This result shows that a small fault (at least 600 m long), oblique with an angle of  $70^\circ$ – $80^\circ$  to the main  $N20^\circ$  Blausasc fault, was activated during the crisis. If we observe in details the spatial and temporal distribution of small events, we can see that they do not follow a particular scheme (Fig. 12). Note that the two main shocks (magnitude 3.2 and 3.0) belong to this family. It is then very difficult to know on which of the two structures they occurred. We will see below that the focal solutions could not help us with this discrimination.

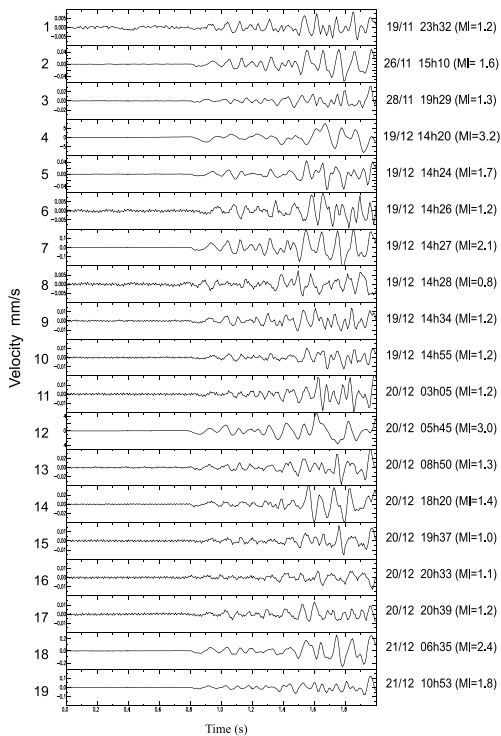


**Figure 10.** Vertical seismograms recorded on station ROCA for all the events of family 1. The location of station ROCA is shown in Fig. 8.

Family 2 contains earthquakes that occurred during a very short period of time (90 min) and very close together in the south of the area. Their relative relocation gives little improvement and groups them into a small zone of about 100 m radius. Family 3 regroups events that occurred in 2000 November in the northern part of the fault segment. They were too few to show any significant alignment and the relative relocation did not group them significantly.

Fig. 8(c) shows the relative relocations of the earthquakes that belong to these families. We used their relative relocation and kept the family barycentre.

#### 4.4 Focal mechanisms

We calculated the focal mechanisms of the four largest events using the polarity of *P* waves on 14–19 stations well distributed in azimuth (Table 1, Figs 8a and 13). The strike slip solutions obtained are stable with depth. Note that the three focal mechanisms numbered 1, 2 and

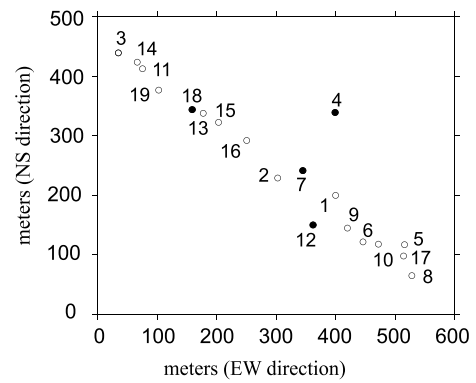


**Figure 12.** Details of the horizontal distribution of events of family 1 after relocation. The numbers refer to Fig. 10 and follow a chronological order.

4 in Table 1 correspond to three events of the same family and that, therefore, they should be almost identical.

For smaller events, we could not find stable focal solutions because they were recorded by too few stations. To nevertheless obtain better constrained solutions, we calculated composite focal mechanisms for the earthquakes of the three families determined before by cross-correlation methods. The similarities of the earthquake waveforms in each family ensure us that their focal mechanisms were highly similar. This approach enabled us to obtain three well-constrained solutions for the 32 events of the three families (Fig. 8c).

For almost all solutions (except for event 3) we retrieved an almost vertical plane oriented N20° to N40° that is in good agreement with the general trend of seismicity during the Blausasc sequence and a left lateral strike slip movement. The other nodal plane was mostly oriented N120°–N130°. This plane was in good agreement with the linear trend highlighted by the relative relocation of the events of family 1.

### 5 TECTONIC INTERPRETATION

During the Blausasc sequence, the major structure activated showed a trend of N20° and the faulting along the Blausasc fault extends from 3 km in depth up to 0.5 km in depth (Fig. 8a and b). In the morphology, the seismic alignment corresponds to the N20° direction of the Paillon valley (Fig. 3).

The present-day seismic sequence did not rupture the surface. Even if the seismicity was very shallow, field investigation in the Paillon valley did not reveal any recent traces of faulting, which is not surprising given the small magnitudes of the largest events of the Blausasc swarm.

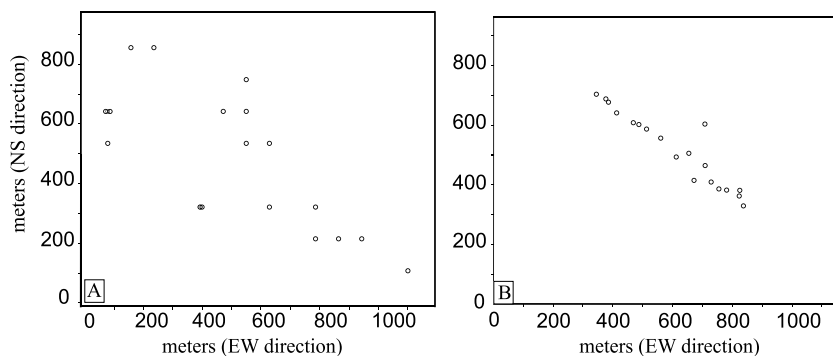


**Figure 11.** (a) Absolute location and (b) relative relocation of the earthquakes of family 1.

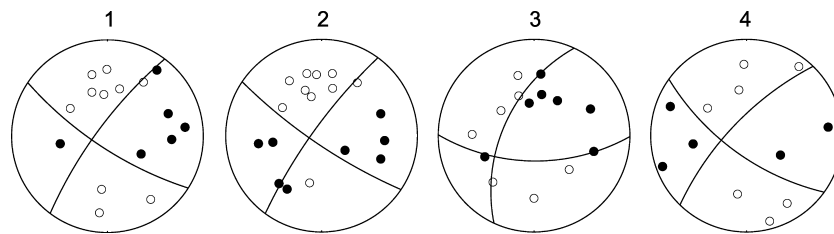


**Figure 13.** Focal solution of the largest events of the crisis. The numbers refer to Fig. 8(a) and Table 1.

The closest fault, the Peille-Laghet fault, is located about 2.5 km to the East of the Blausasc seismic swarm and showed a subparallel trend to the seismic alignment found there (Figs 3 and 8a). The Peille-Laghet fault is around 15 km long. It cross-cuts the sedimentary cover in a  $N20^\circ$  strike and dips  $70^\circ W$ . Its geological evolution is complex: from normal faulting during the Cretaceous extensional phase (Dardeau 1988; De Graciansky & Lemoine 1988) to left-lateral strike-slip faulting during the Miocene compressional phases that involved the emplacement of the Nice arc (Malavieille & Ritz 1989; Ritz 1992). However, field and aerial photographic investigations showed no evidence of morphotectonic anomalies that would suggest Holocene activity of that fault.

Therefore, does a relationship exist between the seismicity and the faults mapped at the surface? The traces of the fault at the surface are part of the Nice arc that was decoupled from the crystalline basement during the major compressional phase (8–5 Ma) with the SSE thrusting of the sedimentary cover. If we take into account the 4–5 km displacement in a  $N170^\circ$  direction, the palaeoposition of the Peille-Laghet fault is approximately on top of the Blausasc seismic alignment (Courboux *et al.* 2003).

We have explored different solutions (e.g. strong bending of a single fault plane, two parallel faults, a flower structure) to explain the relationships between the present-day seismicity pattern and the regional tectonic evolution. Finally, we propose the following hypothesis (Fig. 14): (1) the Peille-Laghet normal fault developed during the Cretaceous times and (2) in late Miocene–Pliocene times, the compressional thin-skin tectonics led to the southward thrusting of the sedimentary cover. During this period, the inherited Peille-Laghet fault was reactivated: the upper part of the fault, which affects the sedimentary cover, was unrooted from its basement and reactivated as a lateral ramp by left-lateral faulting, whereas its basement part remained mainly inactive. In our interpretation, the Peille-Laghet fault has been inactive since the end of the Miocene–Pliocene thrusting. At present, faulting in the basement propagates in the sedimentary cover, delineating the Blausasc fault, under the Paillon valley but without reaching the surface.

## 6 SIMULATION OF A LARGER EVENT ON THE BLAUSASC FAULT

One objective of a seismic hazard analysis is to be able to predict the ground motions due to a future earthquake. This is especially important in regions where no large event has been recorded yet by seismological networks, like the south east of France. We propose in this paragraph to show how, in the region studied, the recordings of small events can be used to simulate a larger earthquake following an empirical Green's function approach (Hartzell 1978).

During the Blausasc sequence, a portion of the recently discovered active Blausasc fault was activated to a length of about 8 km. The larger earthquake that occurred during the Blausasc sequence on this structure had a magnitude  $Ml = 3.2$ , that is, a fault extension

smaller than 1 km, although it is reasonable to think that the fault could generate a larger event (Kafka & Levin 2000). At least if the 8-km portion of the fault activated during the Blausasc sequence had broken in one go, we would expect a magnitude 5.7 earthquake (Wells & Coppersmith 1994).

We decided then to simulate the ground motions that would be generated by such an earthquake in the city of Nice. For this, we used the stochastic summation of empirical Green's functions developed by Kohrs-Sansornny *et al.* (2005). This method requires two input parameters: the moment and the stress drop ratios between the small event and the simulated one. It is well adapted for the simulation of moderate sized earthquakes in low seismicity areas. It has the great advantage of taking into account the path and site effects intrinsically and of reproducing a source model that is coherent with scaling laws. We used the recordings of the  $Ml 3.2$  event of the Blausasc sequence as the empirical Green's function.

We present here the results obtained at two accelerometric stations belonging to the permanent RAP network inside the city of Nice: a station installed on the calcareous hills of the city (NBOR) and a station installed on alluvial deposits in the lower part of the city (NALS). Both time and frequency simulations (elastic response spectra with a damping of 5 per cent) are presented in Fig. 15. For each station, three accelerograms are shown above the 500 simulations realized. The differences between each other are only due to the stochastic method and not to parameters variability. We show, for the elastic response spectra, the results of 10 simulations and the average value over 500 simulations.

The peak ground acceleration (PGA) takes an average value of  $1.5 \text{ m s}^{-2}$  at station NALS, whereas it is smaller than  $0.3 \text{ m s}^{-2}$  for station NBOR. This large difference had been pointed out by previous studies on site effects in this area (Duval 1994; Duval *et al.* 1999; Semblat *et al.* 2000). Note that the duration of vibration is also much longer on NALS than NBOR. This method does not take into account the potential non-linear effects, but it is reasonable to think that they should not be dominant given the relatively small magnitude of the simulated event.

The PGA value of  $1.5 \text{ m s}^{-2}$  obtained in a central part of the city is rather important. If we refer to the parasismic rules actually in application (EPS92), this value should theoretically be supported by recent buildings. Unfortunately, most of the constructions are old, and so, such an earthquake could generate important damage.

It is important to note that the simulation results strongly depend on the static stress drop value chosen for the simulated event (Kohrs-Sansornny *et al.* 2005). In this study, we present only the results obtained under the hypothesis that the static stress drop of the large event is the same than the one of the small event. If we had taken a larger value for the simulated event as it is suggested now by several authors (Beeler *et al.* 2003; Kanamori Rivera 2004), we would have obtained larger values for the accelerations in Nice. A more detailed study on this topic is in progress and will be the subject of another publication.

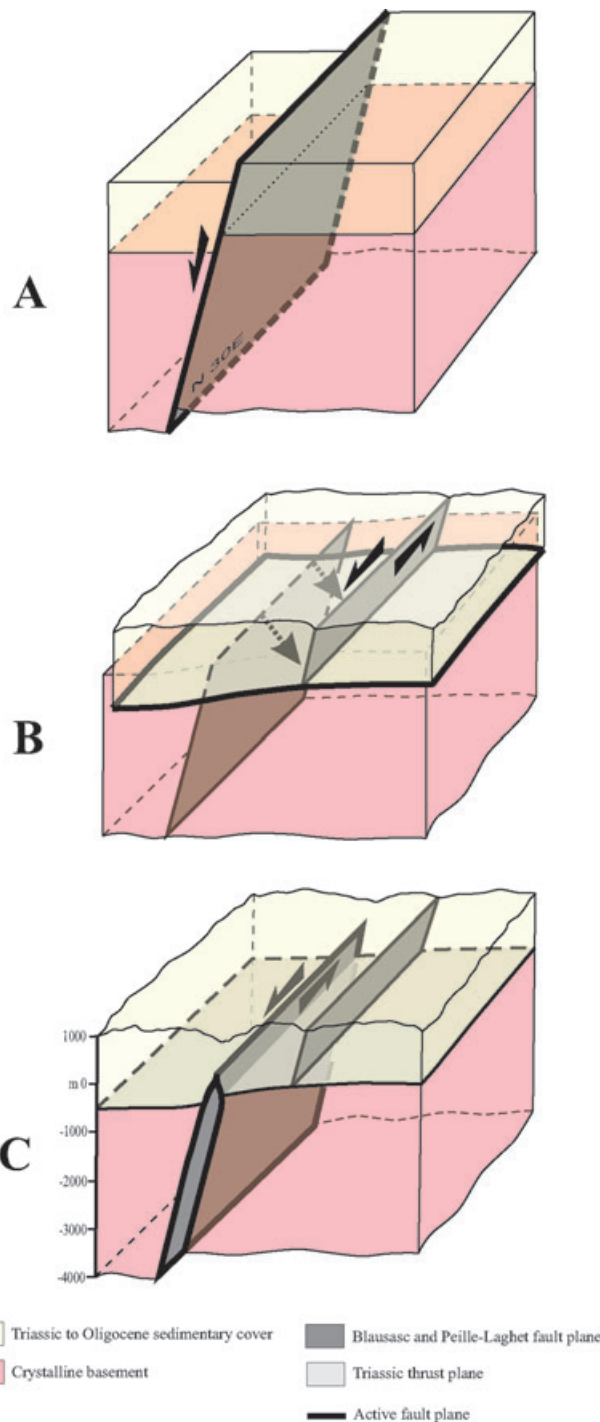


**Figure 14.** 3-D representations of the tectonic evolution of the Blausasc fault from the Cretaceous up to the present-day. (a) Cretaceous extensional faulting; (b) Miocene thin-skin deformations : coupling between N170° thrusting above the basal décollement and left-lateral faulting along the Peille-Laghet fault in the sedimentary cover and (c) Present-day reactivation of the deep part of the fault without propagation of the rupture at surface.

The example of simulation is presented here only to show how new data combined with an appropriated method allows us to obtain realistic simulations of the ground motion that would be generated in the city of Nice by a magnitude 5.7 earthquake occurring on the Blausasc fault.

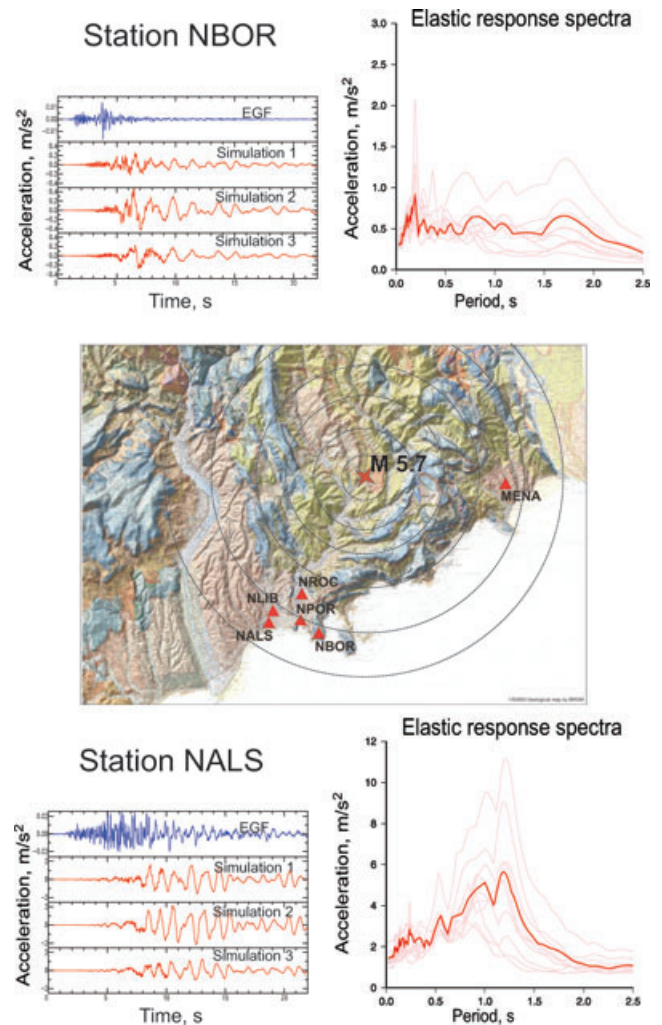


**Figure 15.** Ground motion simulations for a moderate size earthquake ( $M = 5.7$ ) generated on the Blausasc fault, on two stations located in the city of Nice: NBOR is a rocksite station and NALS is situated on alluvial deposits. We present the North-South accelerograms that correspond to the small event taken as Empirical Green's Function (blue line), and three different simulations of the  $M_w = 5.7$  earthquake (red line). The elastic response spectra are shown for 10 different simulations and for the average value over 500 simulations (bold red line). The stress-drop ratio between the small and the large event is taken equal to 1.

## 7 SYNTHESIS AND DISCUSSION

Due to the combination of absolute location and relative relocation, we have shown the existence of two until-now-unknown structures. The larger one (8 km long) trends N20° with a 70° dip to the west, and the smaller one (600 m long) trends N120°.

Referring to the long-term deformation of the region, left-lateral strike-slip faulting along N–NE fractures appears to be the dominant mechanism of deformation in this area. This is attested by the main alignment of epicentres of the 2000 December sequence, by the mechanism of the 1999 November event (Courboulex *et al.* 2001), and by the Peille-Laghet fault plane striations (Larroque *et al.* 2001). This tectonic regime is consistent with the strike-slip faulting stress field determined by Madeddu *et al.* (1997) and Baroux *et al.* (2001) SE of the Argentera Massif, with a NNW–SSE trending  $\sigma_1$  axis. Nevertheless, although the N120° direction does not correspond to

major structures in the field, it is also very interesting because it fits the direction of the small alignment of earthquakes revealed by the relative relocation of the earthquakes of family 1 (Fig. 8c). These two families of earthquake alignments display a pattern of fractures formed by a simple shear deformation regime (e.g. Sylvester 1988, and inset on Fig. 8c): the main shear trends N20° and the antithetic Riedel fractures trends N120°. Consequently, we conclude that both planes have certainly been activated in the meantime or successively during the sequence.

Both faults were activated during the Blausasc sequence but we could not identify without doubt which of them generated the two main events. We tried here to detect an eventual directivity effect of the main shock rupture process that could help us to choose which fault was responsible for the main event. We tried first to invert the near field waveforms of the closest broad-band stations by a non-linear method (B. Delouis, personal communication, 2004), and then to apply an empirical Green's function deconvolution method (Courboulex *et al.* 1999). Unfortunately, neither of these methods gave us a reliable result.

One other interesting feature of this seismic sequence is the migration of seismicity that was observed. Indeed, events migrated from the North in 2000 November to the South in 2000 December. They went across a 1-km-wide gap that could be due to the presence of a barrier (Das & Aki 1977), transmitting stresses without slipping, or an asperity (Lay & Kanamori 1981), aseismically slipping. The smaller N120° fault was not active at the beginning of the Blausasc sequence and appears to have been activated by the conjugated N20° structure. Therefore, we are faced with the stress transfer problem between faults.

The energy repartition indicates that the Blausasc sequence is not a classical main shock-aftershock sequence. It could be a swarm (Scholtz 2002), and the influence of fluids could be important in this case. Indeed, the precipitation during the 2 months (2000 October, November) preceding the Blausasc sequence was four to five times greater than the monthly averages over the last 35 yr (Chamoux 1997). Nevertheless, the *b* value that was seen to be close to 1 (Fig. 7a) is not in good agreement with observations in many other studies that have shown unusually large *b* values when the presence of fluids is important (Scholtz 1968; Sykes 1970).

On a regional scale, the western part of the southern subalpine ranges, the Durance fault and the Trévaresse fault, display some very different features compared to the Blausasc fault, despite a similar state of stress (Baroux *et al.* 2001) and a similar geological setting (Sébrier *et al.* 1997; Chardon & Bellier 2003). For instance, the Moyenne Durance fault (located 150 km west of Nice) is probably the most active fault in the recent past. It is characterized by four historical earthquakes (MSK intensity > VII) since 1509 (Levret *et al.* 1994), and by palaeoseismic events that produced more than one meter of reverse faulting displacement between 27 000 and 9000 BP (Sébrier *et al.* 1997). The instrumental seismicity is low in the area of Durance and Trévaresse, and the present-day deformation rate measured by geodesy is higher in the Nice arc (Ferhat *et al.* 1998; Calais *et al.* 2000). Therefore, the historical seismicity and palaeoseismic events are stronger and more numerous in the West than in the Blausasc area. Is this an indication that the next major earthquake in the southern alpine ranges could occur along the Blausasc fault or a neighbouring fault? This remark also refers to the seismic cycle, which remains a questionable theory in such a region of low deformation rate and strong structural heritage.

## 8 CONCLUSIONS

The new data collected during this experiment are important for seismic hazard estimation. First of all, this experiment points out that in such a region, a large part of the microseismicity cannot be detected and precisely located by permanent networks. Only a very dense seismic network allows us to underline the active structures.

Despite the difficulties in understanding the relationships between the tectonic evolution and the present-day seismic pattern in a complex geological area with low deformation rate, the results of the SALAM experiment allowed us to identify a new active fault, called the Blausasc fault. We propose that this active fault, set in the crystalline basement, is now hidden by the décollement of the sedimentary cover that occurred 8–5 Ma during the emplacement of the Nice arc. It attests that in the setting of fold and thrust belts there is not necessarily a direct relationship between the faults mapped at the surface and the potential seismic sources. It also highlights the importance of inherited structures in a complex intraplate surrounding.

The Blausasc fault is located at only 10 km from densely populated cities like Nice and Monaco and must be taken into account for seismic hazard assessment. These data enabled us to estimate what the ground acceleration could be in two points of the city of Nice if an earthquake of magnitude 5.7 occurs on this fault. The acceleration values obtained using the stochastic empirical Green's function summation method leads us to believe that such a moderate event would have important consequences on the French Riviera. It is important to remind oneself that the strong motion simulation presented in this study corresponds to a case where only the part of the fault that is known is activated, and that there is the possibility of having a much larger event in this zone. The consequences of such an earthquake would be dramatic, especially if cities are not prepared for such a catastrophe.

## ACKNOWLEDGMENTS

We first thank S. Vidal for his role in the data acquisition. We thank Y. Hello and A. Anglade for their involvement in the marine part of the study. We also thank D. Baumont, S. Gaffet, B. Hustedt, A. Lomax, B. Marcaillou, T. Monfret, J-M Noquet, C. Pambrun, R. Pillet, C. Vallet and M. Vergnolle for their help during the field experiment, and E. Calais, B. Delouis and C. Beauval for fruitful discussions. This paper has been enhanced thanks to the remarks of Emmanuel Baroux and an anonymous reviewer. This work was funded by PNRN, ACI Catnat and MEDD thought RDT program. Publication no. 865 of Géosciences Azur.

## REFERENCES

- Arthaud, F. & Matte, P., 1975. Les décrochements tardi-hercynien du Sud-Ouest de l'Europe. Géométrie et essai de reconstitution des conditions de la déformation, *Tectonophysics*, **25**, 139–171.
- Bakun, W. & Scotti, O., 2004. Regional intensity attenuation models for France and the estimation of magnitude and location of historical earthquakes. SCF-4, XXIX General Assembly of the European Seismological Commission, P6271, GFZ Postdam.
- Baroux, E., Béthoux, N. & Bellier, O., 2001. Analyses of the stress field in southeastern France from earthquake focal mechanisms, *Geophys. J. Int.*, **145**, 336–348.

- Beeler, N.M., Wong, T.F. & Hickman, S.H., 2003. On the expected relationships between apparent stress, static stress drop, effective shear fracture energy and seismic efficiency, *Bull. Seism. Soc. Am.*, **93**, 1381–1389.
- Bertil, D., Béthoux, N., Campillo, M. & Massinon, B., 1989. Modeling crustal phases in southeast France from focal depth determination, *Earth Planet. Sci. Lett.*, **95**, 341–358.
- Bogdanoff, S., Michard, A., Poupeau, G. & Mansour, M., 2000. Apatite fission track analysis in the Argentera massif: evidence of contrasting denudation rates in the external crystalline massifs of the western alps, *Terra Nova*, **12**, 117–125.
- Bossolasco, M., Cicconi, G., Eva, C. & Pascale, V., 1972. La rete sismica dell'Istituto Geofisico di Genova e primi risultati sulla sismotettonica delle Alpi Marittime Occidentale e del Mar Ligure, *Riv. Ital. Geofis.*, **21**(5–6), 229–247.
- Bulard, P.F. *et al.*, 1975. Sur la genèse des structures de l'Arc de Nice, *Bull. Soc. Géol. de France*, **XVII**(7), 6,939–944.
- Calais, E. *et al.*, 2000. Crustal strain in the southern Alps, France, 1948–1998, *Tectonophysics*, **319**, 1–17.
- Calais, E., Nocquet, J.M., Jouanne, F. & Tardy, M., 2002. Current extension in the central part of the western Alps from continuous GPS measurements, 1996–2001, *Geology*, **30**(7), 651–654.
- Chamoux, C., 1997. *Structure spatiale des précipitations sur les Alpes Maritimes aux échelles mensuelle et annuelle. Mémoire de Maîtrise de Géographie Physique*, Université de Nice-Sophia Antipolis, 100 pp.
- Chardon, D. & Bellier, O., 2003. Geological boundary conditions of the 1909 Lambesc (Provence, France) earthquake: structure and evolution of the Trévaresse ridge anticline, *Bull. Soc. Géol. Fr.*, **174**(5), 497–510.
- Courboux, F., Deichmann, N. & Gariel, J.C., 1999. Rupture Complexity of a moderate intraplate earthquake in the Alps: the 1996 M5 Epagny-Annecy Earthquake, *Geophys. J. Int.*, **139**, 152–160.
- Courboux, F., Duval, A.M., Deschamps, A., Lomax, A. & Larroque, C., 2001. All the small Peille (Alpes Maritimes, France) earthquake can teach us, *C. R. Acad. Sc. Paris*, **333**, 105–112.
- Courboux, F., Larroque, C., Deschamps, A., Gélis, C., Charreau, J. & Stéphane, J.F., 2003. An unknown active fault revealed by microseismicity in the south-east of France, *Geophys. Res. Lett.*, **30**(15), 1782, doi:10.1029/2003GL017171.
- Dardeau, G., 1988. Tethyan evolution and alpine reactivation of Jurassic extensional structures in the French “Alpes Maritimes”, *Bull. Soc. Géol. de France*, **4**(8), 651–657.
- Das, S. & Aki, K., 1977. Fault planes with barriers : a versatile earthquake model, *J. Geophys. Res.*, **82**, 5658–5670.
- Debran-Passard, S., Courboux, S. & Lienhardt, M.J., 1984. Synthèse géologique du Sud-Est de la France. Mémoire BRGM Fr. n° 125, 615 pp.
- De Graciansky, P.C. & Lemoine, M., 1988. Early Cretaceous extensional tectonics in the southwestern French Alps : a consequence of North Atlantic rifting during Tethyan spreading, *Bull. Soc. Géol. de France* (8), **IV**(5), 733–737.
- De Graciansky, P.C., Dardeau, G., Lemoine, M. & Tricart, P., 1989. The inverted margin of the French Alps and foreland basin inversion, Inversion Tectonics, *Geol. Soc. Spec. Publ.*, **44**, 87–104.
- DeMets, C., Gordon, R., Argus, D. & Stein, S., 1994. Effect of recent revisions to the geomagnetic reversal time scale on estimates of current plate motions, *Geophys. Res. Lett.*, **21**, 2191–2194.
- Dercourt, J. *et al.*, 1986. Geological evolution of the Tethys belt from Atlantic to Pamirs since the Lias, *Tectonophysics*, **123**, 241–315.
- Dewey, J., Helman, M., Turco, E., Hutton, D. & Knott, S., 1989. Kinematics of the western Mediterranean, in *Alpine Tectonics*, Vol. **45**, pp. 265–283, eds M. Coward, D. Dietrich & G. Parks, Geol. Soc. Spec. Publ.
- Duval, A.-M., 1994. Détermination de la réponse d'un site aux séismes à l'aide du bruit de fond, *PhD thesis*, Université Pierre et Marie Curie, Paris, France.
- Duval, A.-M., Méneroud, J.-P. & Vidal, S., 1999. La méthode “H/V bruit de fond” et ses applications aux études d'effet de site, *Monographies d'Etudes et Recherches du réseau des LPC 96–97*, pp 22–25 (document n°502 897), LCPC Publisher, Paris, France.
- Edel, J.B., Dubois, D., Marchant, R., Hernandez, J. & Cosca, M., 2001. La rotation miocène inférieure du bloc corso-sarde; nouvelles contraintes paléomagnétiques sur la fin du mouvement, *Bull. Soc. Géol. Fr.*, **172**(3), 275–283.
- Eva, E. & Solarino, S., 1998. Variations of stress directions in the western Alpine arc, *Geophys. J. Int.*, **135**, 438–448.
- Eva, C. & Rabinovich, A.B., 1997. The February 23, 1887 tsunami recorded on the Ligurian coast, western Mediterranean, *Geophys. Res. Lett.*, **24**, 2211–2214.
- Ferhat, G., Feigl, K., Ritz, J.F. & Souriau, A., 1998. Geodetic measurement of tectonic deformation in the southern Alps and Provence, France, 1887–1994, *Earth Planet. Sci. Lett.*, **159**, 35–46.
- Ferrara, G. & Malaroda, M., 1969. Radiometric age of granitic rocks from the Argentera massif (Maritime Alps), *Boll. Soc. Geol. It.*, **88**, 311–320.
- Ferrari, G., 1991. The 1887 Ligurian earthquake: A detailed study from contemporary scientific observations, *Tectonophysics*, **193**, 131–139.
- Fréchet, J., 1985. Sismogénèse et doublets sismiques. Thèse d'Etat, Univ. Sci. Technol. Médic. Grenoble, 207 pp., *PhD thesis*.
- Gauberti, P., 1973. Peille, son histoire (3 tomes), unpublished book.
- Gèze, B., 1960. La genèse néogène de l'arc de Nice. C.R. somm. Soc. Géol. de France, 33–34.
- Grellet, B., Combes, P., Granier, T. & Philip, H., 1993. *Sismotectonique de la France métropolitaine*, Mémoire H.S. Soc. Géol. de France, 164, 1, 76 pp.
- Got, J.L., Fréchet, J. & Klein, F.W., 1994. Deep fault plane geometry inferred from multiplet relative relocation beneath the south flank of Kilauea, *J. Geophys. Res.*, **99**(B8), 15 375–15 386.
- Gutenberg, R. & Richter, C.F., 1944. Frequency of earthquakes in California, *Bull. Seismol. Soc. Am.*, **90**(3), 185–188.
- Hartzell, S., 1978. Earthquakes aftershocks as Green's functions, *Geophys. Res. Lett.*, **5**, 1–4.
- Haskov, J. & Ottenmøller, L., 1999. SEISAN earthquake analysis software, *Seismol. Res. Lett.*, **70**, 532–534.
- Kanamori, H., & Rivera, L., 2004. Static and dynamic scaling relations for earthquakes and their implications for rupture speed and stress drop, *Bull. Seismol. Soc. Am.*, **94**, 314–319.
- Hoang Trong, P., Haessler, H., Holl, J.M. & Legros, Y., 1987. L'essai sismique (Oct. 83–Jan. 84) de la moyenne vallée de la Roya (Alpes Maritimes): Activité récente d'un ancien système de failles conjuguées?, *C.R. Acad. Sci. Paris*, **304**, 419–424.
- Kafka, A.L. & Levin, S.Z., 2000. Does the spatial distribution of smaller earthquakes delineate areas where larger earthquakes are likely to occur?, *Bull. Seismol. Soc. Am.*, **90**(3), 724–738.
- Kerckhove, C., 1969. La “zone du Flysch” dans les nappes de l'Embrunais-Ubaye (Alpes Occidentales), *Géol. Alpine*, **45**, 1–202.
- Kohrs-Sansorny, C., Courboux, F., Bour, M. & Deschamps, A., 2005. A two-stage method for ground-motion simulation using stochastic summation of small earthquakes, *Seismol. Soc. Am.*, **95**, 1387–1400.
- Lambert, J. & Levret, A., 1996. *Mille ans de séismes en France*, Ouest Editions Presses Académiques, Nantes, 120 pp.
- Larroque, C. *et al.*, 2001. Active deformation at the junction between southern French Alps and Ligurian basin, *Netherlands J. Geosci.*, **80**, 255–272.
- Laurent O., Stéphane, J.F. & Popoff, M., 2000. Modalités de la structuration miocène de la branche sud de l'arc de Castellane (chaînes subalpines méridionales), *Géologie de la France*, **3**, 33–65.
- Lay, T. & Kanamori, H., 1981. An asperity model of great earthquake sequences. in *Earthquake Prediction, an International Review; M. Ewing Ser. 4*, pp. 579–592, eds D. Simpson & P. Richards, American Geophysical Union, Washington, DC
- Levret, A., Backe, J.C. & Cushing, M., 1994. Atlas of macroseismic maps for French earthquakes with their principal characteristics, *Nat. Haz.*, **10**, 19–46.
- Maddedu, B., Béthoux, N. & Stéphane, J.F., 1997. Champ de contrainte post-pliocène et déformations récentes dans les Alpes sud-occidentales, *Bull. Soc. Géol. de France*, **167**(6), 797–810.
- Malaroda, R., Carraro, F., Dal Piaz, G., Franceschetti, B., Sturani, C., & Zanella, E., 1970. Carta geologica del Massiccio dell'Argentera alla scala 1/50 000, *Note illustrative Mem. Soc. Geol. It.*, **9**, 557–663.

- Malavieille, J. & Ritz, J.F., 1989. Mylonitic deformation of evaporites in décollements: examples from Southern Alps, *France. J. Struct. Geol.*, **11**, 583–590.
- Marini, M., 1987. Le deformazioni fragili del Pliocene Ligure; implicazioni nella geodinamica Alpina, *Mem. Soc. Geol. Ital.*, **29**, 157–169.
- McKenzie, D., 1969. The relation between fault plane solutions for earthquakes and the directions of the principal stresses, *Bull. Seism. Soc. Am.*, **59**, 591–601.
- Montigny, R., Edel, J.B. & Thuziat, R., 1981. Oligo-Miocene rotation of Sardinia: K-Ar and paleomagnetic data of tertiary volcanics, *Earth Planet. Sci. Lett.*, **54**, 261–271.
- Mueller, B., Zoback, M.L., Fucks, K., Mastin, L., Gregersen, S., Pavoni, N., Stephansson, O. & Ljunggreen, C., 1992. Regional patterns of tectonic stress in Europe, *J. Geophys. Res.*, **97**, 11 783–11 803.
- Nocquet, J.M. & Calais, E., 2003. Crustal velocity field of Western Europe from permanent GPS array solutions, 1996–2001, *Geophys. J. Int.*, **154**, 72–88.
- Pauchet, H., Rigo, A., Rivera, L. & Souriau, A., 1999. A detailed analysis of the February 1996 aftershock sequence in the eastern Pyrenées, France, *Geophys. J. Int.*, **137**, 107–127.
- Perez, J.L., 1975. La zone limite entre l'arc de Nice et l'arc de la Roya (Alpes Maritimes). Observations structurales. *Bull. Soc. Géol. de France*, **XVII**(7), 930–938.
- Perrot, J. et al., 2005. Analysis of the Mw 4.3 Lorient earthquake sequence: a multidisciplinary approach to the geodynamics of the Armorican Massif, westernmost France, *Geophys. J. Int.*, **162**, 935–950.
- Rebai S., Philip H & Taboada, A., 1992. Modern tectonic stress field in the Mediterranean region : evidence for variation in stress direction at different scales, *Geophys. J. Int.*, **110**, 106–140.
- Riccou, L.E. & Siddans, A., 1986. Collision tectonics in the western Alps, in *Collision Tectonics*, pp. 229–244, eds. M. Coward & A.C. Ries, Geol. Soc. Spec. Publ., 19.
- Ritz, J.F., 1992. Tectonique récente et sismotectonique des Alpes du Sud, analyse en terme de contraintes, *Quaternaire*, **3**, 111–124.
- Rollet, N., Déverchère, J., Beslier, M.O., Guennoc, P., Réhault, J.P., Sosson, M. & Truffert, C., 2002. Back arc extension, tectonic inheritance and volcanism in the Ligurian Sea, western Mediterranean, *Tectonics*, **21**(3), doi:10.1029/2001TC900027.
- Scholtz, C.H., 1968. The frequency-magnitude relation of microfracturing in rock and its relation to earthquakes, *Bull. Seismol. Soc. Am.*, **58**, 399–415.
- Scholtz, C.H., 2002. *The Mechanics of Earthquakes and Faulting*, 2nd edn, 471 pp, Cambridge University Press, Cambridge, United Kingdom.
- Scotti, O. & Levret, A., 2000. How to calculate seismic parameters for large offshore historical earthquakes, Abstracts, ESC XXVII general assembly, Lisbon, Portugal, 10–15 September 2000 40.
- Sébrier, M., Ghafiri, A. & Blès, J.L., 1997. Paleoseismicity in France: fault trench studies in a region of moderate seismicity, *J. Geodyn.*, **24**, 207–217.
- Sella, G.F., Dixon, T.H. & Mao, A., 2002. REVEL: A model for recent plate velocities from space geodesy, *J. Geophys. Res.*, **107**(B4), doi: 10.1029/2000JB000033.
- Semblat, J-F., Duval, A.-M. & Dangla, P., 2000. Numerical analysis of seismic wave amplification in Nice (France) and comparisons with experiments, *Soil Dyn. Earthquake Eng.*, **19**, 347–362.
- Siddans, A., 1979. Arcuate fold patterns in the subalpine chains of Southeast France, *J. Struct. Geol.*, **1**, 117–126.
- Sisfrance Historical Data Base, <http://www.sisfrance.net/>.
- Souriau, A., Sylvander M, Rigo, A., Fels, J.F., Douchain, J.M. et Ponsolles, C. (2001). Sismotectonique des Pyrénées: principales contraintes sismologiques, *Bull. Soc. Géol. France*, **172**(1), 25–39.
- Sykes, L.R., 1970. Earthquake swarms and sea-floor spreading, *J. Geophysic. Res.*, **75**, 6598–6611.
- Sylvester, A., 1988. Strike-slip faults, *Geol. Soc Am. Bull.*, **100**, 1666–1703.
- Thouvenot, F., Frechet, J., Jenatton, L. & Garmond, J.F., 2003. The Belledone border Fault: Identification of an active seismic strike-slip fault in the western Alps, *Geophys. J. Int.*, **155**, 174–192.
- Tricard, P., 1984. From passive margin to continental collision: a tectonic scenario for the western Alps, *Am. J. Sci.*, **284**, 97–120.
- Vigny, C. et al., 2002. GPS network monitors the western Alps: deformation over a five-year period: 1993–1998, *J. Geodesy*, **76**, 63–76.
- Wells, D.L. & Coppersmith, K.J., 1994. New empirical relationships among magnitude, rupture length, rupture width, rupture area, and surface displacement, *Bull. Seismol. Soc. Am.*, **84**, 974–1002.
- Working Group CPTI, 1999. Catalogo Parametrico dei Terremoti Italiani, ING, GNDT, SGA, SSN, Compositori Eds, Bologna, 1999, ISBN 88-7794-201-0, 92 pp.